

ChemComm

Accepted Manuscript



This is an *Accepted Manuscript*, which has been through the Royal Society of Chemistry peer review process and has been accepted for publication.

Accepted Manuscripts are published online shortly after acceptance, before technical editing, formatting and proof reading. Using this free service, authors can make their results available to the community, in citable form, before we publish the edited article. We will replace this *Accepted Manuscript* with the edited and formatted *Advance Article* as soon as it is available.

You can find more information about *Accepted Manuscripts* in the [Information for Authors](#).

Please note that technical editing may introduce minor changes to the text and/or graphics, which may alter content. The journal's standard [Terms & Conditions](#) and the [Ethical guidelines](#) still apply. In no event shall the Royal Society of Chemistry be held responsible for any errors or omissions in this *Accepted Manuscript* or any consequences arising from the use of any information it contains.

COMMUNICATION

www.rsc.org/

Cite this: DOI: 10.1039/x0xx00000x

Highly Efficient Mesoscopic Solar Cell Based on $\text{CH}_3\text{NH}_3\text{PbI}_{3-x}\text{Cl}_x$ via Sequential Solution Deposition

Received 00th January 2012,

Accepted 00th January 2012

DOI: 10.1039/x0xx00000x

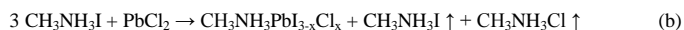
Yingzhuang Ma,^a Lingling Zheng,^a Yao Shien Chung,^a Saisai Chu,^a Lixin Xiao,^{a,b*} Zhijian Chen,^{a,b} Shufeng Wang,^{a,b} Bo Qu,^{a,b} Qihuang Gong,^a Zhaoxin Wu,^{c*} and Xun Hou^c

A mixed halide perovskite of $\text{CH}_3\text{NH}_3\text{PbI}_{3-x}\text{Cl}_x$ is synthesized via two-step sequential solution deposition by using a mixture of PbCl_2 and PbI_2 as the precursor to overcome the low solubility of pure PbCl_2 with easy morphology control. 11.7% of power conversion efficiency is achieved for the mesoscopic cell, much higher than the cell via spin-coating process.

Hybrid perovskite materials with the form of AMX_3 ($\text{A} = \text{CH}_3\text{NH}_3^+$; $\text{M} = \text{Pb}^{2+}$, or Sn^{2+} ; and $\text{X} = \text{Cl}^-$, Br^- , or I^-) was first discovered by Weber and developed by Mitzi et al., and then $\text{CH}_3\text{NH}_3\text{PbI}_3$ or $\text{CH}_3\text{NH}_3\text{PbBr}_3$ were used as the dye-absorbing layer in a liquid dye-sensitized solar cell (DSC) initiated by Miyasaka et al.¹⁻³ Following the pioneering work, the perovskites were used in solid-state solar cells to avoid the dissolution of perovskite in the presence of liquid electrolyte. As a result, much higher power conversion efficiencies (PCEs) were achieved than those liquid cells.⁴⁻²² Recently, Snaith et al. found that the electron-hole diffusion lengths exceeded $1 \mu\text{m}$ for the mixed halide perovskite of $\text{CH}_3\text{NH}_3\text{PbI}_{3-x}\text{Cl}_x$, while it was only 100 nm for the triiodide perovskite of $\text{CH}_3\text{NH}_3\text{PbI}_3$, showing the promising prospects of $\text{CH}_3\text{NH}_3\text{PbI}_{3-x}\text{Cl}_x$.⁸ The mixed halide perovskite $\text{CH}_3\text{NH}_3\text{PbI}_{3-x}\text{Cl}_x$ achieved 15.4% of PCE through mix-vapor vacuum deposition to give a uniform perovskite film with a planar heterojunction.¹⁰ However, vacuum deposition will greatly increase the cost of large-scale fabrication than the cost-effective solution process. Up to now, spin-coating deposition is widely used for the fabrication of solution-based $\text{CH}_3\text{NH}_3\text{PbI}_{3-x}\text{Cl}_x$ cells, but only 7.6% of PCE for the $\text{CH}_3\text{NH}_3\text{PbI}_{3-x}\text{Cl}_x$ cell containing mesoporous TiO_2 layer.⁴ While $\text{CH}_3\text{NH}_3\text{PbI}_3$ devices with shorter diffusion lengths achieved the efficiencies over 15% by two-step sequential solution deposition, with easier morphology control.^{7,22} The morphology of the resultant perovskite film is very sensitive to the conditions during the spin-coating procedure, e.g., thickness of the compact TiO_2 layer, annealing time, annealing temperature and the thickness of the perovskite layer.¹⁵ The morphology of the perovskite is crucial to the device performance, because the defects in perovskite crystallites and the interfaces may be the trap of charges, preventing them reaching the electrodes. Therefore, it is necessary to improve the morphology of $\text{CH}_3\text{NH}_3\text{PbI}_{3-x}\text{Cl}_x$ cell through the solution-based method.

To further improve the photovoltaic performance of mixed halide perovskite of $\text{CH}_3\text{NH}_3\text{PbI}_{3-x}\text{Cl}_x$ via solution process, in this work, we successfully figure out the feasible compositions of the precursor for the $\text{CH}_3\text{NH}_3\text{PbI}_{3-x}\text{Cl}_x$ perovskite by two-step sequential deposition, permitting much easier morphology control. A mixture precursor of PbI_2 and PbCl_2 is more promising for the preparation of $\text{CH}_3\text{NH}_3\text{PbI}_{3-x}\text{Cl}_x$ than pure PbCl_2 , due to the poor solubility of pure PbCl_2 . The device performance reaches to 11.7%, which is the highest efficiency for $\text{CH}_3\text{NH}_3\text{PbI}_{3-x}\text{Cl}_x$ via solution process containing mesoporous TiO_2 layer based our knowledge, much higher than 4.8% for the device fabricated via spin-coating deposition.

The $\text{CH}_3\text{NH}_3\text{PbI}_{3-x}\text{Cl}_x$ perovskite was first reported by Snaith et al. by using a mixture of $\text{CH}_3\text{NH}_3\text{I}$ and PbCl_2 with a molar ratio of 3:1 via spin-coating deposition (Scheme 1b).^{4,5,8} Following this reaction, we first tried to use saturated (0.5 M) PbCl_2 as the precursor in the two-step sequential deposition, and spin-coated it on the mesoporous TiO_2 film, and then dipped into $\text{CH}_3\text{NH}_3\text{I}$ solution to form perovskite on site. Unfortunately, the absorption of the resultant film was very weak. It might be due to the poorer solubility of PbCl_2 than that of PbI_2 in dimethylformamide (DMF), because high concentration (at least 1 M) of the precursor is very important to obtain high loading in the mesoporous TiO_2 film for high device performance.⁷ However, in the presence of additives, e.g., PbI_2 or $\text{CH}_3\text{NH}_3\text{I}$, the solubility of PbCl_2 can be significantly increased due to the common ion effect.^{15,31} In addition, the higher formation energy of chlorine incorporation into the perovskite matrix than that of iodine might also be the reason.²⁶ Therefore, we changed the precursor to a mixture of 0.5 M PbCl_2 and 0.5 M PbI_2 (molar ratio 1:1) according to the reaction of Scheme 1a, and followed the two-step sequential deposition to give **Film a** with the color changing from chartreuse to dark brown, indicating the formation of the perovskite. From the reaction formula given below, it could also be inferred that Scheme 1a tends to give less byproducts compared to Scheme 1b. The excess methylammonium iodide and chloride are assumed to be lost via evaporation during the annealing process.⁴ Less byproducts may leave fewer pin-holes in the perovskite layer during the annealing process.¹⁵ As comparison, the resultant film formed by using PbCl_2 as the precursor (Scheme 1b) is referred as **Film b**. The illustrations of different fabrication procedures for $\text{CH}_3\text{NH}_3\text{PbI}_{3-x}\text{Cl}_x$ layers are shown in Figure 1.



Scheme 1. The reactions for the $\text{CH}_3\text{NH}_3\text{PbI}_{3-x}\text{Cl}_x$.

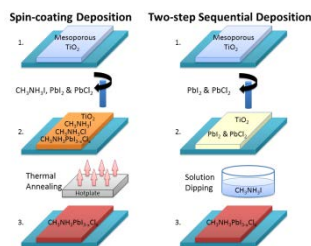


Figure 1. The illustrations of fabrication procedures of perovskite layer via spin-coating deposition and two-step sequential deposition.

The structures of the resultant perovskite films were investigated via X-ray diffraction (XRD) as shown in Figure 2a. The structure of the synthesized perovskite is well consistent with tetragonal phase structures as the previous report.²³⁻²⁵ Strong peaks at 14.03° and 27.52° , corresponding to the (110) and (220) planes, confirm the formation of a tetragonal perovskite structure with lattice parameters $a = b = 8.84 \text{ \AA}$ and $c = 12.57 \text{ \AA}$. The signals of **Film b** are much weaker than those of **Film a**, indicating more perovskite crystallites formed in mesoporous TiO_2 by the mixture of PbI_2 and PbCl_2 than pure PbCl_2 as the precursor. The composition of **Film a** was confirmed by energy-dispersive x-ray (EDX) spectrum as shown in Figure S1. The elemental mapping analysis of the surface confirms that the resultant perovskite of **Film a** is mixed halide $\text{CH}_3\text{NH}_3\text{PbI}_{3-x}\text{Cl}_x$ with approximate $x \approx 0.26$. The images of Pb, I and Cl also show that the perovskite are well distributed. The absorption spectra of the two perovskite films were shown in Figure 2b. **Film a** has strong broadband absorption in the visible region from 400 nm to 800 nm, on the contrary, **Film b** has rather poor absorption, indicating insufficient perovskite filling in the porous TiO_2 layer. These results indicate that using the mixture of PbI_2 and PbCl_2 as the precursor is an effective way to form the mixed halide perovskite of $\text{CH}_3\text{NH}_3\text{PbI}_{3-x}\text{Cl}_x$, following Scheme 1a.

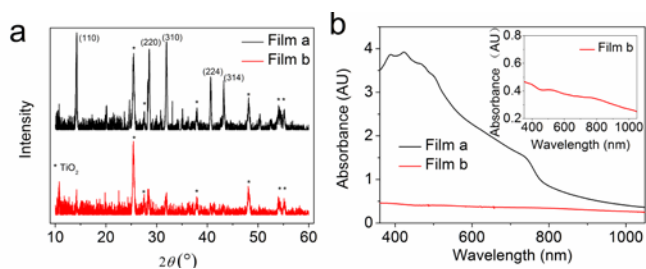


Figure 2. a) XRD spectra of **Film a** and **b**. b) Absorbance of **Film a** and **b**.

To further evaluate the differences of the resultant $\text{CH}_3\text{NH}_3\text{PbI}_{3-x}\text{Cl}_x$ perovskite layers between two-step sequential deposition and spin-coating deposition, we also fabricated another perovskite layer via spin-coating the mixture of $\text{CH}_3\text{NH}_3\text{I}$, PbCl_2 and PbI_2 (molar ratio 2:1:1) also following Scheme 1a for comparison (hereafter referred as **Film c**). The morphology of **Film a**, **Film b** and **Film c** were measured by both scanning electron microscopy (SEM) and atomic force microscope (AFM) as shown in Figure 3.

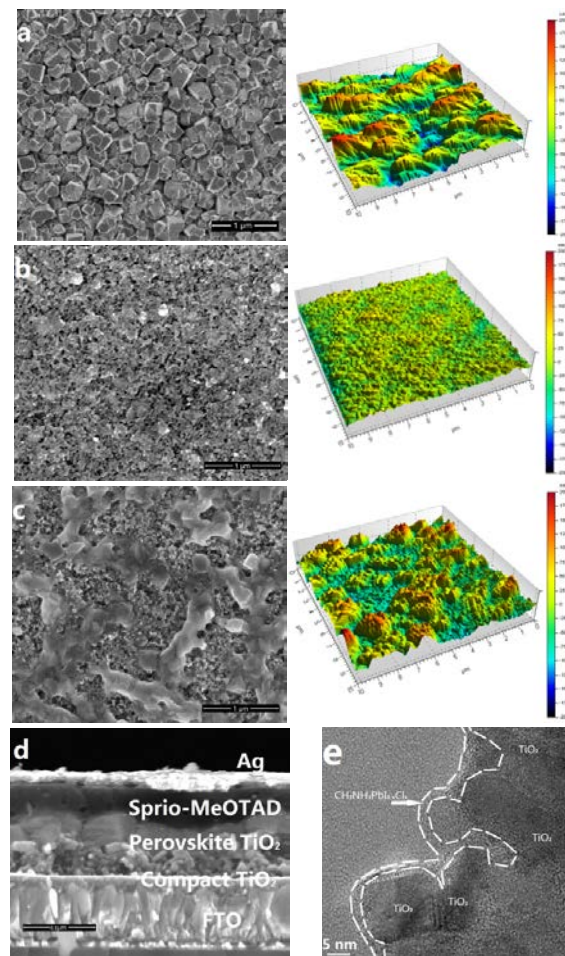


Figure 3. The SEM and AFM images of a) **Film a**, b) **Film b** and c) **Film c**. d) The cross-section SEM view of **Device A**. e) TEM images of $\text{CH}_3\text{NH}_3\text{PbI}_{3-x}\text{Cl}_x$ deposited in the mesoporous TiO_2 film.

By using the mixture of PbI_2 and PbCl_2 as the precursor (**Film a**), the perovskite via two-step sequential deposition did not only penetrate deeply into the mesoporous TiO_2 , but also grew into crystallites to cover the TiO_2 layer with in-plane grain size of 300 ~ 350 nm as shown in Figure 3a, and the grain size has been proved to be suitable with strong light scattering effect to further enhance the light absorption.³⁰ On the contrary, there was almost no more perovskite crystallites on top of the mesoporous TiO_2 for **Film b** via two-step sequential deposition by using PbCl_2 as the precursor as shown in Figure 3b, indicating insufficient pore filling in the mesoporous TiO_2 layer. This might be one of the possible reasons for the absorption difference by using different precursors. For **Film c**, the SEM images (Figure 3c) showed that no continuous perovskite capping layer was formed on top of the mesoporous TiO_2 , although there was penetration into the mesoporous TiO_2 layer. These above results indicate that the morphology of perovskite layer via two-step sequential deposition is easier to control compared with via spin-coating deposition. The surface morphology of the three films was also performed via AFM images. As a result, the crystalline arrangement in **Film a** formed a continuous microstructure consistent with the SEM image, the absorption of incident light was enhanced due to the presence of the crystalline perovskite capping layer and the light scattering effect, which have also been proved to be an effective way in DSCs.^{22,27} These results could be proved by the cross-section image (Figure 3d) with elemental mapping (Figure

S2) of **Film a**. It could be clearly identified that the perovskite not only formed continuous capping layer, but also penetrated well into the mesoporous TiO₂ film. The perovskite pore-filling should improve the device performance because higher electron densities can be sustained in the TiO₂ layer, increasing electron transporting rates as previously reported.²⁸ To further evaluate the interfacial properties of TiO₂/perovskite, the transmission electron microscopy (TEM) image (Figure 3e) was obtained from the scratch from **Film a**. The image reveals the formation of the CH₃NH₃PbI_{3-x}Cl_x perovskite thin film on the TiO₂ surface, which prohibits the direct contact between TiO₂ and hole transporting material (HTM).

The experimental details of device fabrication are given in the Supplementary Information. **Device A** and **B** correspond to **Film a** and **Film c**, respectively. Devices were measured under standard AM 1.5 illumination of 100 mW/cm². The *J-V* curves were shown in Figure 4a. The incident photon to current conversion efficiency (IPCE) was measured as shown in Figure 4b.

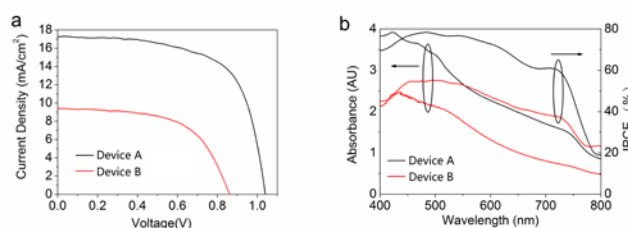


Figure 4. a) The photovoltaic performances of **Device A** and **B**. b) Absorbance and IPCE of the perovskite films in **Device A** and **B**.

Table 1. Photovoltaic performances of the hybrid perovskite solar cells.

Device	Process	V_{oc} [V]	J_{sc} [mA/cm ²]	FF	PCE [%]
A	Sequential	1.04	17.2	0.65	11.7
B	Spin-coating	0.86	9.4	0.59	4.8
Ref. 10	Vacuum	1.07	21.5	0.67	15.4
Ref. 4	Spin-coating	0.80	17.8	0.53	7.6

Compared with **Device B**, the IPCE of **Device A** is over 60% between 400 to 700 nm, and the highest value is near 80% at around 500 nm, matches the stronger absorption region of the perovskite layer. The PCE of **Device A** is up to 11.7%, with J_{sc} of 17.2 mA/cm², V_{oc} of 1.04 V, and FF of 0.65, which is the highest efficiency for CH₃NH₃PbI_{3-x}Cl_x via solution process containing mesoporous TiO₂ layer based our knowledge, much higher than that of 7.6% via spin-coating process with the mesoporous TiO₂ layer as reported listed in Table 1.⁴ The corresponding **Device B** showed a J_{sc} of 9.4 mA/cm², V_{oc} of 0.86 V, FF of 0.59 and 4.8% of PCE (Figure 5a), much lower PCE than that of the **Device A** fabricated via two-step sequential deposition. The improvement of photovoltaic performances may be mainly ascribed to the different perovskite morphology in the two devices. Compared with **Device A**, there is 0.18 V of decreasing in **Device B** on V_{oc} because of the direct contact between the uncovered TiO₂ and the *p*-type HTM due to the absence of the perovskite capping layer, resulting in the charge recombination between the TiO₂ and HTM.^{15,28,29} Besides, the absence of the perovskite capping layer might lead to lower absorption, resulting in lower J_{sc} . It should be noted here that the lower PCE than 15% for CH₃NH₃PbI₃ via two-step sequential deposition might be due to the lower solubility of PbCl₂ than that of PbI₂ in the solvent of DMF. High concentration should be crucial to the growing of perovskite crystallites as reported in the case of CH₃NH₃PbI₃ via two-step sequential deposition.⁷ This could be also supported by the fact of lower PCEs for CH₃NH₃PbI_{3-x}Cl_x via solution process than that via vacuum deposition (sufficient

chlorine source). Compared to the CH₃NH₃PbI_{3-x}Cl_x cell with 15.4% of PCE via vacuum deposition, the V_{oc} and the FF of the spin-coated CH₃NH₃PbI_{3-x}Cl_x cells is significantly lower, due to the difficulty to control the morphology of the perovskite crystallites via spin-coating process, leading to the lower PCE of 7.6%. While, **Device A** fabricated via two-step sequential deposition is an effective method to reduce the V_{oc} and FF losses caused by the morphology defects of CH₃NH₃PbI_{3-x}Cl_x perovskite. Further work should be focused on optimizing the condition to controlling the morphology of the perovskite capping layer to further increase the lower J_{sc} caused by the low solubility of PbCl₂ as mentioned above.

Conclusions

In conclusion, we introduce two-step sequential solution deposition for the fabrication of CH₃NH₃PbI_{3-x}Cl_x mesoscopic solar cell. The mixture of PbI₂ and PbCl₂ is used rather than pure PbCl₂ as the precursor to ensure high loading in the mesoporous TiO₂ film, with easy morphology control, which results in a great enhancement of the light absorbance for the device and suppressing the electron hole recombination by separating the bare TiO₂ and the HTM layer. As a result, 11.7% of PCE for the device has been achieved with 17.2 mA/cm² of J_{sc} , 1.04 V of V_{oc} , and 0.65 of FF , which is the highest efficiency for CH₃NH₃PbI_{3-x}Cl_x via solution process containing mesoporous TiO₂ layer based our knowledge. This is much higher than 4.8% for the device fabricated via spin-coating process. This work suggests a promising way for the solution-based preparation of the mixed halide perovskite of CH₃NH₃PbI_{3-x}Cl_x for highly efficient solar cells.

This study was partly financially supported by the National Natural Science Foundation of China (10934001, 61177020, 11074016, 11121091, 61275034 and 61106123) and the National Basic Research Program of China (2013CB328700). The authors are thankful to Mr. Xiao Yu and Prof. Dechun Zou in the College of Chemistry and Molecular Engineering of Peking University for their kindly help in the assistance in the measurements of SEM images.

Notes and references

^a State Key Laboratory for Mesoscopic Physics and Department of Physics, Peking University, Beijing 100871, PR China. E-mail: xiao66@pku.edu.cn

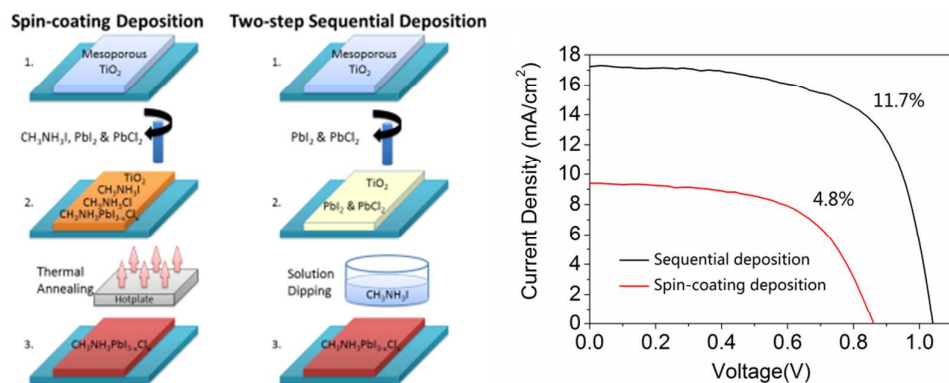
^b New Display Device and System Integration Collaborative Innovation Center of the West Coast of the Taiwan Strait, Fuzhou 350002, China

^c Key Laboratory of Photonics Technology for Information, Key Laboratory for Physical Electronics and Devices of the Ministry of Education, Department of Electronic Science and technology, School of Electronic and Information Engineering, Xi'an Jiaotong University, Xi'an, 710049, PR China. E-mail: zhaoxinwu@mail.xjtu.edu.cn

† Electronic Supplementary Information (ESI) available: The Supplementary Information includes material synthesis, EDX results, device preparation procedures, and device characterization. See DOI: 10.1039/c000000x/

1. D. Weber, *Z. Naturforsch. B* 1978, **33**, 1443.
2. D. B. Mitzi, C. A. Field, W. T. A. Harrison, and A. M. Guloy, *Nature* 1994, **369**, 467.
3. A. Kojima, K. Teshima, Y. Shirai, and T. Miyasaka, *J. Am. Chem. Soc.* 2009, **131**, 6050.

4. M. M. Lee, J. Teuscher, T. Miyasak, T. N. Murakami, and H. J. Snaith, *Science* 2012, **338**, 643.
5. J. M. Ball, M. M. Lee, A. Hey, and H. J. Snaith, *Energy Environ. Sci.* 2013, **6**, 1739.
6. H. S. Kim, C. R. Lee, J. H. Im, K. B. Lee, T. Moehl, A. Marchioro, S. J. Moon, R. H. Baker, J. H. Yum, J. E. Moser, M. Grätzel, and N. G. Park, *Sci. Rep.* 2012, **2**, 591.
7. J. Burschka, N. Pellet, S. J. Moon, R. Humphry-Baker, P. Gao, M. K. Nazeeruddin, and M. Grätzel, *Nature* 2013, **499**, 316.
8. S. D. Stranks, G. E. Eperon, G. Grancini, C. Menelaou, M. J. Alcocer, T. Leijtens, and H. J. Snaith, *Science* 2013, **342**, 341.
9. G. Xing, N. Mathews, S. Sun, S. S. Lim, Y. M. Lam, M. Grätzel, and T. C. Sum, *Science* 2013, **342**, 344.
10. M. Liu, M. B. Johnston, and H. J. Snaith, *Nature* 2013, **501**, 395.
11. L. Etgar, P. Gao, Z. Xue, Q. Peng, A. K. Chandiran, B. Liu, and M. Grätzel, *J. Am. Chem. Soc.* 2012, **134**, 17396.
12. D. Bi, L. Yang, G. Boschloo, A. Hagfeldt, and E. M. Johansson, *J. Phys. Chem. L.* 2013, **4**, 1532.
13. D. Sabba, H. M. Kumar, N. Yantara, T. T. T. Pham, N. G. Park, M. Grätzel, and P. P. Boix, *Nanoscale* 2014, **6**, 1675.
14. M. H. Kumar, N. Yantara, S. Dharani, M. Grätzel, S. Mhaisalkar, P. P. Boix, and N. Mathews, *Chem. Comm.* 2013, **49**, 11089.
15. G. E. Eperon, V. M. Burlakov, P. Docampo, A. Goriely, and H. J. Snaith, *Adv. Funct. Mater.* 2014, **24**, 151.
16. J. Y. Jeng, Y. F. Chiang, M. H. Lee, S. R. Peng, T. F. Guo, P. Chen, and T. C. Wen, *Adv. Mater.* 2013, **25**, 3727.
17. J. H. Heo, S. H. Im, J. H. Noh, T. N. Mandal, C. S. Lim, J. A. Chang, and S. I. Seok, *Nature Photonics* 2013, **7**, 486.
18. H. S. Kim, J. W. Lee, N. Yantara, P. P. Boix, S. A. Kulkarni, S. G. Mhaisalkar, and N. G. Park, *Nano Lett.* 2013, **13**, 2412.
19. A. Abrusci, S. D. Stranks, P. Docampo, H. L. Yip, A. K. Y. Jen, and H. J. Snaith, *Nano Lett.* 2013, **13**, 3124.
20. N. G. Park, *J. Phys. Chem. L.* 2013, **4**, 2423.
21. J. Burschka, A. Dualeh, F. Kessler, E. Baranoff, N. L. Cevey-Ha, C. Yi, and M. Grätzel, *J. Am. Chem. Soc.* 2011, **133**, 18042.
22. D. Liu, and T. L. Kelly, *Nature Photonics* 2014, **8**, 133.
23. T. Baikie, Y. Fang, J. M. Kadro, M. Schreyer, F. Wei, S. G. Mhaisalkar, and T. J. White, *J. Mater. Chem. A* 2013, **1**, 5628.
24. C. C. Stoumpos, C. D. Malliakas, and M. G. Kanatzidis, *Inorg. Chem.* 2013, **52**, 9019.
25. S. Colella, E. Mosconi, P. Fedeli, A. Listorti, F. Gazza, F. Orlandi, P. Ferro, T. Besagni, A. Rizzo, G. Calestani, G. Gigli, F. D. Angelis, and R. Mosca, *Chem. Mater.* 2013, **25**, 4613.
26. E. Mosconi, A. Amat, M. K. Nazeeruddin, M. Grätzel, and F. D. Angelis, *J. Phys. Chem. C* 2013, **117**, 13902.
27. S. Hore, P. Nitz, C. Vetter, C. Prah, M. Niggemann, and R. Kern, *Chem. Commun.* 2005, **15**, 2011.
28. T. Leijtens, B. Lauber, G. E. Eperon, S. D. Stranks, and H. J. Snaith, *J. Phys. Chem. Lett.* 2014, **5**, 1096.
29. H. J. Snaith, N. C. Greenham and R. H. Friend, *Adv. Mater.*, 2004, **16**, 1641.
30. Q. Chen, H. Zhou, Z. Hong, S. Luo, H.-S. Duan, H.-H. Wang, Y. Liu, G. Li and Y. Yang, *J. Am. Chem. Soc.*, 2013, **136**, 622.
31. Mendham, J.; Denney, R. C.; Barnes, J. D.; Thomas, M. J. K. (2000), *Vogel's Quantitative Chemical Analysis* (6th ed.), New York: Prentice Hall, ISBN 0-582-22628-7



A mixed halide perovskite of $\text{CH}_3\text{NH}_3\text{PbI}_{3-x}\text{Cl}_x$ is synthesized via two-step sequential solution deposition by using a mixture of PbCl_2 and PbI_2 as the precursor to overcome the low solubility of pure PbCl_2 with easy morphology control. 11.7% of power conversion efficiency is achieved for the mesoscopic cell, much higher than the cell via spin-coating process.